Nanoscale

PAPER

View Article Online
View Journal | View Issue



Cite this: Nanoscale, 2022, 14, 7364

# Patchy metal nanoparticles with polymers: controllable growth and two-way self-assembly†

Hanyi Duan, [a] Tessa Malesky,[b] Janet Wang,[b] Chung-Hao Liu,[a] Haiyan Tan,[c] Mu-Ping Nieh, [a,c] Yao Lin *[a,b,c] and Jie He *[a,b,c]

Received 2nd March 2022,
Accepted 14th April 2022

DOI: 10.1039/d2nr01221a

rsc.li/nanoscale

We report a new design of polymer-patched gold nanoparticles (AuNPs) with controllable interparticle interactions in terms of their direction and strength. Patchy AuNPs (pAuNPs) are prepared through hydrophobicity-driven surface dewetting under deficient ligand exchange conditions. Using the exposed surface on pAuNPs as seeds, a highly controllable growth of AuNPs is carried out via seed-mediated growth while retaining the size of polymer domains. As guided by ligands, these pAuNPs can self-assemble directionally in two ways along the exposed surface (head-to-head) or the polymer-patched surface of pAuNPs (tail-to-tail). Control of the surface asymmetry/coverage on pAuNPs provides an important tool in balancing interparticle interactions (attraction vs. repulsion) that further tunes assembled nanostructures as clusters and nanochains. The self-assembly pathway plays a key role in determining the interparticle distance and therefore plasmon coupling of pAuNPs. Our results demonstrate a new paradigm in the directional self-assembly of anisotropic building blocks for hierarchical nanomaterials with interesting optical properties.



## 1. Introduction

There has been remarkable progress in controlled synthesis of metal nanoparticles (NPs) with a variety of shapes, sizes, and chemical composition.[1–3] These metal NPs as building blocks provide tremendous opportunities in design of functional materials using bottom-up self-assembly.[4–14] Synthesis favors symmetry to lower the surface energy under given synthetic conditions;[15] however, self-assembly benefits from asymmetry.[16–18] Adding asymmetry to NP building blocks has a significant impact on interparticle interactions that guides and potentially programs self-assembly in a specific pathway. Using truncated tetrahedral quantum dots as an example, asymmetric surface ligand modification on their $(10\bar{1}1)$ and (0002) facets led to the formation of quasicrystalline superlattices with a 10-fold rotational symmetry.[19] Reducing or breaking the symmetry on the surface of NPs, therefore, provides directional interparticle interactions to guide the self-assembly of NPs in an unprecedented way. To this end, one area that has drawn increasing interest is the selective ligand modification of metal NPs to form the so-called patchy NPs.[20,21] Ligands can pattern the surface of NPs through a number of methods, including templated surface modification,[22,23] site-specific grafting,[24–26] phase separation of mixed ligands,[27–31] and hydrophobicity-driven phase segregation.[32,33] As a post-synthetic method, surface ligands pattern the surface of metal NPs having pre-designed nanostructures without re-designing and re-synthesizing of NPs. When grafting hydrophobic polymers on plasmonic metal NPs, hydrophobicity-driven surface dewetting has proved to anisotropically pattern the NP surface as demonstrated by Kumacheva,[32] Nie[34] and us.[35,36] When transferred from a good to a selective solvent, hydrophobic polymer ligands show a transition from isotropic (core–shell) to anisotropic (patched) coating on metal NPs, namely surface dewetting.[37] As a result, distinct properties between the covered and exposed NP surfaces can potentially provide directional interparticle interactions to assemble patchy NPs.[25] While asymmetric patches with various chemical compositions can guide self-assembly as reported recently,[38–40] there is very limited controllability over the balance of attractive and repulsive interparticle interactions that play a key role in determining the self-assembly outcomes.

In the current contribution, we report a versatile synthetic strategy to precisely pattern gold NPs (AuNPs) with well-defined ligand coverage and/or topologically asymmetric patches. We further demonstrate the use of asymmetric ligand distribution to guide the self-assembly of patched AuNPs (pAuNPs) in two opposite directions, namely head-to-head (H–H) and tail-to-tail (T–T). The key findings are three-fold.

[a]Polymer Program, University of Connecticut, Storrs, CT 06269, USA. E-mail: yao.lin@uconn.edu, jie.he@uconn.edu
[b]Department of Chemistry, University of Connecticut, Storrs, CT 06269, USA
[c]Institute of Materials Science, University of Connecticut, Storrs, CT 06269, USA

†Electronic supplementary information (ESI) available. See DOI: https://doi.org/10.1039/d2nr01221a

First of all, we resolve the synthetic challenges in controlling surface asymmetry/coverage to balance interparticle interactions. Through the combination of hydrophobicity-driven surface dewetting and seed-mediated growth, the exposed Au surface can further grow with great size precision to tune ligand coverage on pAuNPs stoichiometrically (Scheme 1). Second, these pAuNPs can self-assemble directionally in two ways: along the exposed surface (or H–H) or the polymer-patched surface of pAuNPs (or T–T). By selectively removing the capping ligands or chemically grafting hydrophilic poly (ethylene oxide) (PEO) on the newly grown Au surface, we can switch the two self-assembly pathways (Scheme 1). The two-way self-assembly shows a distinct impact on the interparticle localized surface plasmon resonance (LSPR) coupling. Third, the balance of attractive and repulsive interparticle interactions provides a powerful tool to vary the self-assembly outcomes in both H–H and T–T pathways. With dedicated rebalance of thermodynamic driving forces, the self-assembly kinetics and nanostructures of pAuNPs in each pathway can be controlled. Our results therefore open up enormous new possibilities to design not only symmetry-breaking metal NP building blocks but also their assembly with predictable nanostructures with new ensemble properties.

## 2. Results and discussion

The preparation of initial Janus-type pAuNPs (Fig. 1a) was carried out using a previously reported procedure.[36] In brief, $PS_{200}$-SH ($M_n$ = 20.7 kg mol$^{-1}$, Đ = 1.1) and $PS_{40}$-b-$PEO_{114}$ ($M_n$ = 9.2 kg mol$^{-1}$, Đ = 1.1, Fig. S1†) were dissolved in N,N-dimethylformamide (DMF). A pre-concentrated citrate-capped AuNP solution (14.6 ± 1.3 nm, Fig. S2†) was then added dropwise into the above DMF solution. After gentle shaking, the solution was incubated at room temperature overnight, followed by the addition of deionized water (15 vol% relative to DMF) as a non-solvent to trigger the coil–globule transition of PS. The glass vial was then sealed and annealed at 100 °C for 1 h. After cooling, the formed Janus-type pAuNPs were quenched by injecting the solution into excess water. The pAuNPs were centrifuged three times to remove free polymers. The LSPR peak of pAuNPs is 527 nm in water (Fig. S3†), about 8 nm redshift as compared to original AuNPs. These pAuNPs are very stable in water and no change was seen after one-year storage.

The nanostructure of pAuNPs was first revealed by transmission electron microscopy (TEM, Fig. 1b and c). pAuNPs show typical snowman shapes where the polymer domain forms a micelle-like patch on the surface of AuNPs. AuNPs appear darker than the polymer domains, due to their difference in electron density. The diameter of AuNPs ($d_{Au}$) and the size of polymer micelles ($d_{poly}$, cross with AuNPs) were measured to be 14.8 ± 1.1 nm (Fig. 1f) and 20.3 ± 2.2 nm (Fig. S3†), respectively. Low-resolution TEM confirms the high uniformity of pAuNPs with a yield of >95% for Janus-type patched pAuNP-14 (Fig. S3 and S4†). pAuNP-14 was examined by TEM at different tilted angles (Fig. 1d). The projected polymer domains at high tilted angles (55° and −55°) become crescent and obviously smaller as compared to the projected images at low tilted angles, while the size and shape of AuNPs had a minimum change. This is due to the overlap of AuNPs and polymer domains at high tilted angles which shields the lighter polymer domains. These results confirm the formation of asymmetric polymer coverage on AuNPs. All pAuNPs likely have polymer domains directly dried on the TEM grids because the high-angle images show the flat interface of polymer domains with the grid. The formation of Janus-type pAuNPs is driven by surface dewetting under deficient ligand exchange (DLE) as reported previously.[32,34,36] When transferring from a good solvent to a poor solvent for PS-SH, the collapsed PS ligands de-wetted the surface of AuNPs, leading to the formation of polymer patches in the presence of $PS_{40}$-b-$PEO_{114}$. The surface coverage of AuNPs by the polymer domain, denoted as $A_c$, is ~62% as estimated from TEM (Fig. S5†).

These Janus-type pAuNPs have two distinct surfaces, i.e., the exposed surface (likely capped by citrate, see below) and the covered surface by polymer micelles. Using the seed-mediated growth, metals (or a second metal) can further grow from the exposed surface to tune the $A_c$ while polymer domains remain frozen below the glass transition temperature ($T_g$, ~110 °C). The typical growth solution was prepared by mixing cetrimonium bromide (CTAB), $HAuCl_4$ and ascorbic acid (see details in the ESI†).[41] After adding pAuNP-14 as seeds, the growth was evidenced by the solution color change (Fig. 2g). At an Au equivalence ($Au_{eq}$) of 24 (Au in the growth solution relative to pAuNP-14 nm) to grow pAuNP-38 (Fig. 1c, S6 and Table S1†), upon the mixing of the seed solution and the growth solution, the color turned from light pink to purplish red gradually. As monitored by UV-vis (Fig. 1h), the LSRP for pAuNP-14 seeds peaked at 527 nm and an immediate increase of the peak intensity was seen along with the red shift to 534 nm after 30 s. The LSPR absorbance of pAuNPs kept increasing in the first 5 min, due to the larger molar absorp-

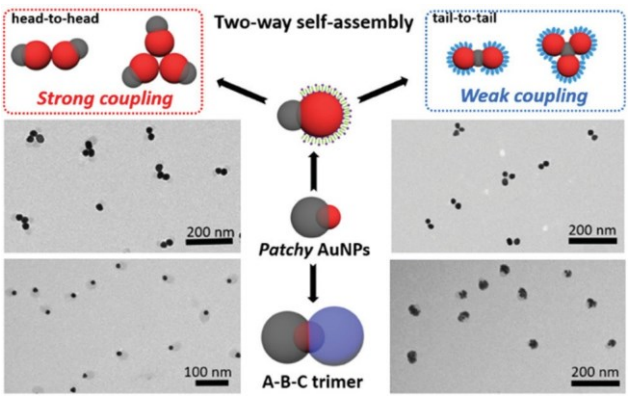


Scheme 1 Preparation and self-assembly of pAuNPs as guided by polymer patches. Representative TEM images: H–H clusters (left top), T–T clusters (right top), pAuNP-14 seeds (left bottom) and Pt@pAuNP-14 hetero trimers (right bottom).

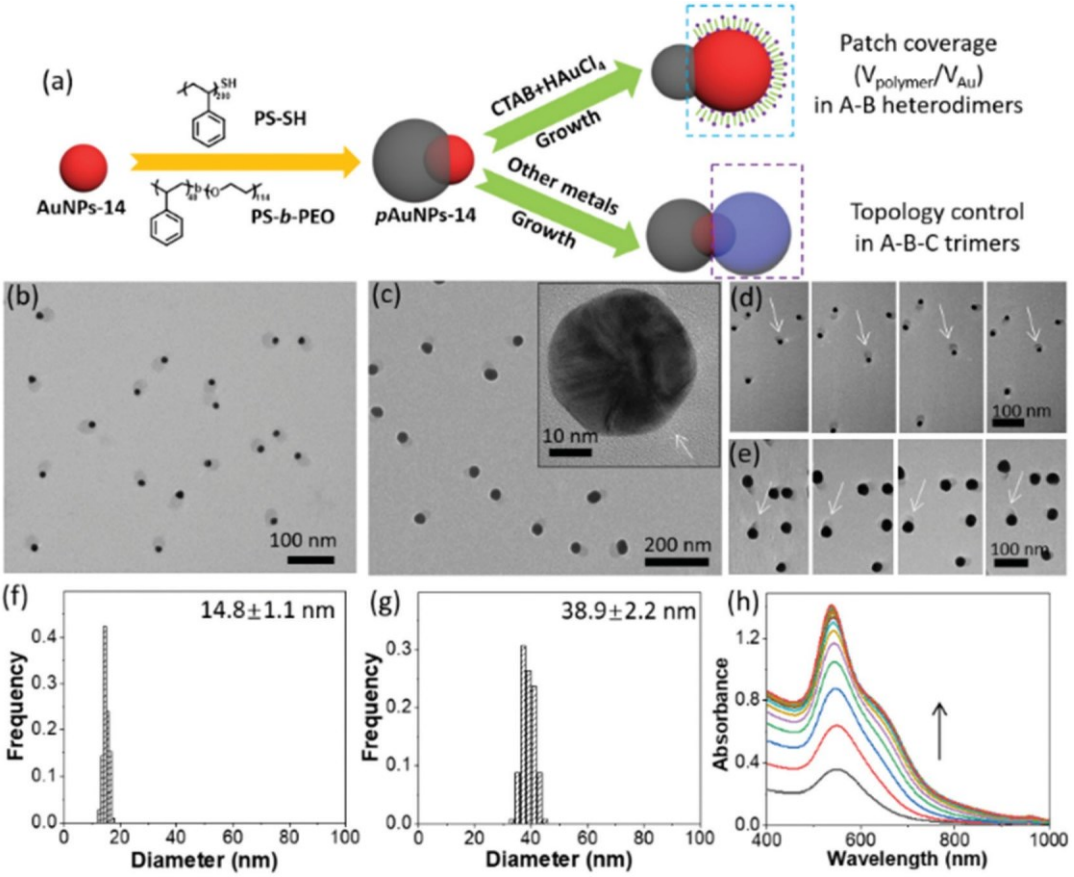


Fig. 1 (a) Scheme illustrating the preparation of pAuNPs and seed-mediated growth to control surface coverages and topologies. (b and c) Low-resolution TEM images of pAuNP-14 (b) and pAuNP-38 (c). The inset in c shows the polycrystalline Au core with an arrow indicating the direction of the polymer patch. TEM images of pAuNP-14 seeds (d) and pAuNP-38 (e) at different tilted angles: −55°, −20°, 20° and 55° (left to right). Histograms of $d_{Au}$ before (f) and after growth (g). (h) In situ UV-vis spectra monitoring the growth of pAuNP-38 nm with a time interval of 30 s.

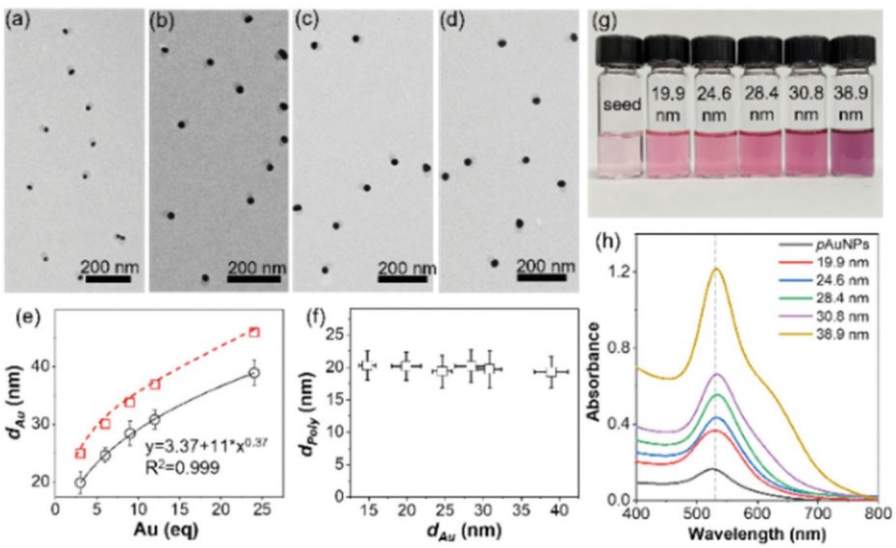


Fig. 2 (a–d) TME images of pAuNPs with different Au sizes: 19.9 ± 1.9 nm (a); 24.6 ± 1.3 nm (b); 28.4 ± 2.1 nm (c); and 30.8 ± 1.6 nm (d). (e) Plotting the diameter of pAuNPs against $Au_{eq}$. Red square: the ideal size with 100% conversion and black circle: the measured size from TEM. (f) Plotting $d_{poly}$ of Janus-type pAuNPs against the diameter of the Au core. (g) Images of pAuNP aqueous solutions with different Au sizes. (h) UV-vis spectra of pAuNPs with different Au sizes.

 

tion coefficient (ε) for larger AuNPs given their constant molar concentration.[42] A new shoulder peak was found at 638 nm after 3 min. This is somewhat different from the size increase of Au due to the layer-by-layer growth, known as the Frank–van der Merwe mechanism, where no shoulder peak is expected for spherical AuNPs with a larger size.[41] The shoulder peak is presumably due to the asymmetric growth of AuNPs along the exposed surface of pAuNPs, leading to the appearance of a dipole resonance mode. Similar LSPR peaks were reported in the formation of Au@Au dimers.[43] The $d_{Au}$ value increases to 38.9 ± 2.2 nm (Fig. 1g), while the size of the polymer domain ($d_{poly}$) is 19.3 ± 2.4 nm (Fig. 2f), comparable to that of pAuNPs-14 seeds.

The seed-mediated growth also provides great precision on the size of freshly grown Au domains by varying $Au_{eq}$. Fig. 2a–d show the TEM images of pAuNPs at various $Au_{eq}$ values. When increasing $Au_{eq}$, a continuous growth of Au domains was observed in the range of 14–38 nm. All these pAuNPs show uniform distribution with a high yield of >90% to Janus-type pAuNPs (Fig. S7–S9†). For example, at $Au_{eq}$ = 6, the $d_{Au}$ value increased to 24.6 nm as pAuNP-24, while the $d_{poly}$ value remained as 19.4 nm. The yield of Janus-type pAuNP-24 nm is close to 95% where only one polymer domain attaches on AuNPs. More quantitatively, the size of Au domains fits well against $Au_{eq}$ through a scaling law, $d_{Au} \propto Au_{eq}^{0.37}$ (Fig. 2e). It is very close to the power law of $Au_{eq}^{0.33}$ assuming the conversion of $HAuCl_4$ to be 100%. These results suggest that the growth of Au domains was mediated and initiated on the exposed surface of pAuNP-14 seeds.

The growth of pAuNPs also has a strong impact on the LSPR absorption of AuNPs. Fig. 2g shows the typical image of pAuNP solutions at different $Au_{eq}$ values. With a larger Au domain, the solution became deeply red. With $d_{Au}$ > 30 nm, the solutions were slightly purplish. The UV-vis spectra of pAuNPs are shown in Fig. 2h. As the concentration of pAuNP-14 remained as 0.288 nM, the peak intensity had an obvious increase with the size of AuNPs. For $d_{Au}$ > 30 nm, pAuNPs show a similar shoulder peak at 634 nm, close to that of pAuNP-38 at a long growth time (Fig. 1h). These results are consistent with the asymmetric growth on pAuNP-14 seeds.

Interestingly, no significant change of polymer domains was seen during the seed-mediated growth (Fig. 2f). The $d_{poly}$ value is approximately 20 nm regardless of the size of Au domains. Polymer domains were likely frozen in water; therefore, the size of freshly grown Au domains that are only covered by CTAB can be independently tuned. Since $d_{poly}$ as well as the polymer–Au interface did not vary, the surface coverage of pAuNPs with polymer ligands ($A_c$) would continuously decrease (Table S2 and Fig. S5†). Qualitatively, the $A_c$ will be propositional to $d_{Au}^{-2}$ (see details in the ESI†). For pAuNP-19, the $A_c$ value is 33%; the $A_c$ value further decreases to 8.7% for pAuNP-38. It is therefore expected that these pAuNPs would have controllable surface ligand composition and coverage.

We further confirm the critical role of the second capping ligand, e.g., CTAB, in the controlled growth of new Au domains during the seed-mediated growth. With a strong capping ligand, like CTAB, cetyltrimethylammonium chloride (CTAC), polyvinylpyrrolidone (PVP), and poly(acrylic acid) (PAA), we observed a similar growth trend of pAuNPs where spherical Au domains were seen after growth (Fig. S10†). In the presence of a weak ligand like citrate, multi elongated Au islands were grown on pAuNP-14 seeds. These Au islands were easily distinguished, and they had smaller interfaces with the original seeds, similar to those obtained without the second capping ligands (Fig. S11†). This presumably is attributed to the fast deposition rate where the weak ligands allow the fast binding and diffusion of adatoms.[44] We measured the UV-vis spectra of pAuNPs grown with different second capping ligands at $Au_{eq}$ = 6. The LSPR peaks of pAuNPs for CTAC, PVP and PAA capped pAuNPs are around 540 nm (Fig. S10†), close to pAuNP-24 nm with CTAB. These LSPR peaks are sharp, indicating the uniformity of newly grown Au domains. However, pAuNPs grown with citrate have two distinct LSPR peaks located at 536 nm and 613 nm, arising from these elongated Au islands.

Our synthetic strategy can be further extended to design other more sophisticated patchy structures on AuNPs, like A–B–C topological heterotrimers with two different patches.[45,46] Noble metals, like Ag (Fig. 3a–c and S12†), Pd (Fig. S13 and S14†) and Pt (Fig. 3d–f and S15†), can be grown on pAuNP-14 seeds.[44] The examples of Ag and Pt domains selectively grown from the exposed Au surface have a yield of >95% and reasonable uniformity. The energy-dispersive X-ray spectroscopy (EDX) mapping and high-angle annular dark-field (HAADF) images confirm the formation of asymmetric coating (Fig. 3). The high-resolution TEM images suggest that (i) Ag and Au have a close interface given the close match of their lattice structures (Fig. 3c) and (ii) Pt domains form as a corona with a porous structure on pAuNP-14 seeds (Fig. 3f) under this specific condition.[45,47]

Surface anisotropy was further used to guide the self-assembly of these NP building blocks. Using pAuNPs as an example, the unique two-way self-assembly in H–H and T–T modes as directionally guided by polymer patches is illustrated in

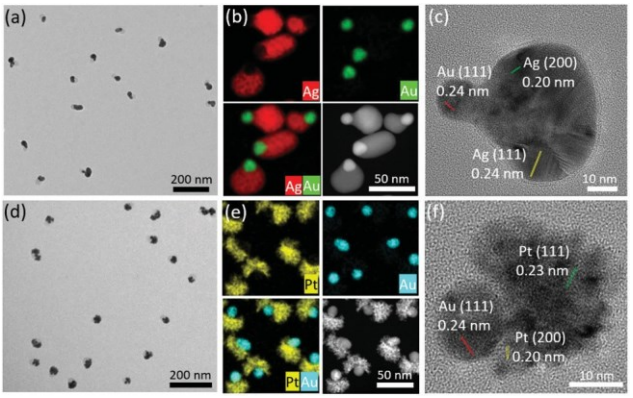


Fig. 3 Low-resolution TEM image (a), EDX mapping and HADDF (b), and high resolution TEM image (c) of Ag@pAuNP-14. Low resolution TEM image (d), EDX mapping and HADDF (e), and high resolution TEM image (f) of Pt@pAuNP-14.

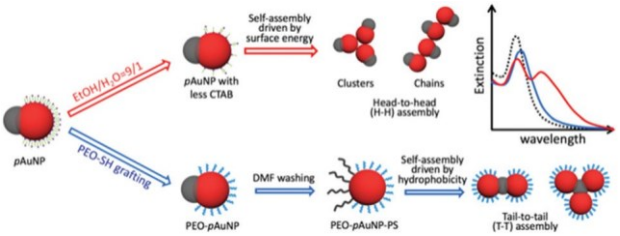


Scheme 2 Two-way self-assembly strategy of pAuNPs: H–H and T–T modes.

Scheme 2. In the H–H mode, we used the van der Waals interactions of the exposed Au surface capped with CTAB. After selective removal of CTAB, pAuNPs form aggregates along the exposed Au surface while the polymer patches stabilize such assemblies.[48] Strong interparticle plasmon coupling is expected since no ligands are in between pAuNPs. In the T–T mode, the exposed Au surface of pAuNPs was further grafted by hydrophilic polymer ligands like $PEO_{44}$-SH. After removal of polymer domains, pAuNPs become amphiphilic where $PEO_{44}$-SH and $PS_{200}$-SH pattern the surface of AuNPs as Janus-type amphiphiles (PEO–pAuNP–PS). In the poor solvent of PS, PEO–pAuNP–PS can assemble in the T–T mode with a weak plasmon coupling due to the large interparticle distance. More importantly, the delicate balance of $A_c$ enables the interaction strength to be controlled, in addition to simply providing directional forces among pAuNPs. It is, therefore, possible to access hierarchical assemblies with directional and controllable interparticle forces.

To trigger the H–H self-assembly, the aqueous solution of pAuNPs was first centrifuged twice to remove excess CTAB. The final pAuNPs were re-dispersed in 0.1 mL of water, followed by adding 0.9 mL of ethanol.[48] The self-assembly was monitored by in situ UV-vis spectroscopy. Using pAuNP-28 nm as an example, a large hump appeared as a shoulder peak in the range of 600–700 nm after incubation for 1 h (Fig. 4b). This shoulder peak grew gradually, and the solution color turned from red to purplish. The peak at 604 nm became much more pronounced at a longer incubation time and no further decrease at 533 nm was seen after 1 h incubation. The self-assembly was quenched by adding excess PVP. We assigned this new UV peak to the strong plasmon coupling of assembled pAuNP-28. A similar trend was found for pAuNPs with different Au sizes (Fig. S18 and S20†); however, the plasmon shift is highly determined by the size of AuNPs.[49] For pAuNP-38 nm, the new peak at 676 nm rose as fast as compared to that of pAuNP-28 nm (Fig. 4c). It took around 3 h to have the comparable peak intensity with the main LSPR peak at 534 nm. As the $A_c$ value decreased, larger pAuNPs had more surfaces capped by CTAB. The removal of CTAB, essentially driven the self-assembly, would theoretically provide stronger interparticle attraction, although larger AuNPs have a slower diffusion in solution. As a control, pAuNP-14 seeds did not show any color change even after 24 h (Fig. 4a), indicating that pAuNP-14 seeds with a high $A_c$ value were stable in an ethanol/water mixture. Note that, the H–H self-assembly of pAuNPs is irreversible and cannot be reversed by changing the ratio of ethanol/water.

Assembled nanostructures of pAuNPs were further examined by TEM. Fig. 4d shows pAuNP-14 seeds incubated in ethanol/water after 24 h. Well-dispersed individual pAuNPs were observed, consistent with the UV-vis result (Fig. 4a). When increasing the Au domains of pAuNPs, there is a clear morphological transition from individual NPs to clusters and eventually to chains (more TEM results in Fig. S16–S22†). The

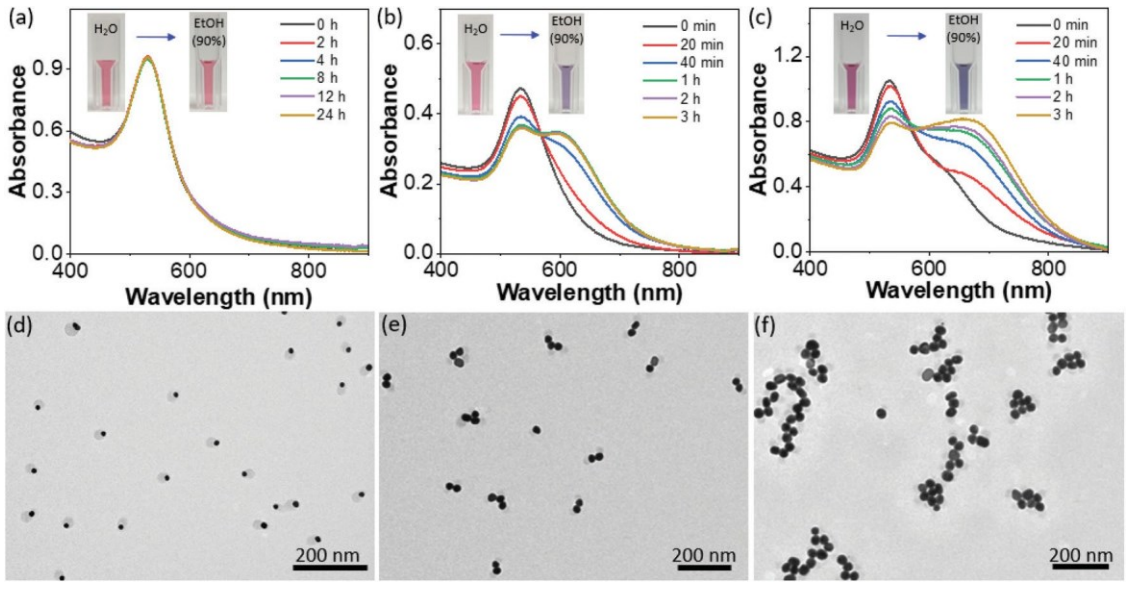


Fig. 4 UV-vis absorption spectra (a–c) and TEM images (d–f) of pAuNP-14 nm (a and d), 28 nm (b and e) and 38 nm (c and f). All experiments were carried out in an ethanol/water mixture (9/1, vol) at room temperature.

 

typical TEM image of assembled pAuNP-28 nm is shown in Fig. 4e. With an $A_c$ value of 16.3%, clusters of pAuNP-28 were seen under TEM. Dimers and trimers are the major products with a total yield of 81% (Fig. S19†). All these clusters have polymer domains facing out to the solvent in order to stabilize these nanoclusters. Notably, there is nearly no interparticle spacing seen from TEM. Adjacent AuNPs were in close contact where the near field coupling of AuNPs is strong, as seen by UV-vis. Further increasing the size of Au domains leads to the formation of larger aggregates that better shields the interface of uncovered Au with the solvent. For pAuNP-38, the dominant assemblies were short nanochains. Among these nanochains, the Au domains of pAuNP-38 formed different packing, including linear chains, zig-zag chains and bundled double chains (see schemes and more images in Fig. S21†), while polymer patches were around the surface of these aggregates.

In the case of T–T self-assembly, the exposed surface of pAuNPs was first modified through ligand exchange with hydrophilic $PEO_{44}$-SH in water.[50] After $PEO_{44}$-SH replaced CTAB, we used DMF to dissolve and further remove free CTAB and $PS_{40}$-b-$PEO_{114}$ through centrifugation (see experimental details in the ESI†). The final pAuNPs were thus patterned asymmetrically with $PEO_{44}$-SH and $PS_{200}$-SH as Janus-type PEO–pAuNP–PS (Scheme 2). As amphiphiles,[51] they can assemble in a selective solvent like water. Fig. 5c and e show the TEM images of PEO–pAuNP–PS assemblies obtained from pAuNP-14 in water. Since pAuNP-14 has an $A_c$ value of 62%, the AuNP surface is largely covered with $PS_{200}$-SH. There is a strong hydrophobicity to drive the self-assembly to form nanochains (~97% of AuNPs in chains). Some chains are very long, up to a few micrometers. These nanochains are very different from the H–H nanochains as given in Fig. 4f. There are clear gaps in between adjacent AuNPs which were filled with $PS_{200}$-SH (see more zoomed-in images in Fig. S23†). The UV-vis results of the T–T nanochains are shown in Fig. 5a. A large and broad LSPR band with a peak at 539 nm was seen. It is similar to that of nanochains formed by PS-grafted AuNPs in the literature.[52–54] It is noteworthy that the T–T self-assembly is reversible. When redispersing these nanostructures in DMF, a good solvent to both PEO and PS, the LSPR peak of pAuNPs can be fully restored. Subsequent dialysis against water would trigger re-self-assembly reversibly, resulting in the formation of T–T assemblies.

The assembled nanostructures of PEO–pAuNP–PS obtained from pAuNP-28 are compared using TEM (Fig. 5d and f). As the $A_c$ value of pAuNP-28 nm reduced to 16.3%, the hydrophobicity of these PEO–pAuNP–PS became weaker. These amphiphilic AuNPs only formed clusters in water. The yield of dimers and trimers is ~65%; while ~29% of AuNPs did not assemble as measured from TEM (Fig. S24†). Under TEM, lighter polymer domains formed by hydrophobic $PS_{200}$-SH are also visualizable (Fig. 5b). Among these clusters, the gap between AuNPs is around 4.2 nm. These results confirm, again, that the T–T assemblies were formed along the AuNP surface grafted with $PS_{200}$-SH. The LSPR peak of these clusters appeared at 542 nm (Fig. 5b), in good agreement with our TEM observation. The larger LSPR shift as compared to that of nanochains (Fig. 5a) is presumably due to the size increase of AuNPs. In addition, for A–B–C heterotrimers, similar T–T assemblies could be designed using the hydrophobicity of PS. Pt@pAuNP-14 as an example formed more complicated clusters along the surface covered by PS where Pt domains covered by PVP were at the ends to stabilize these clusters (Fig. S25†).

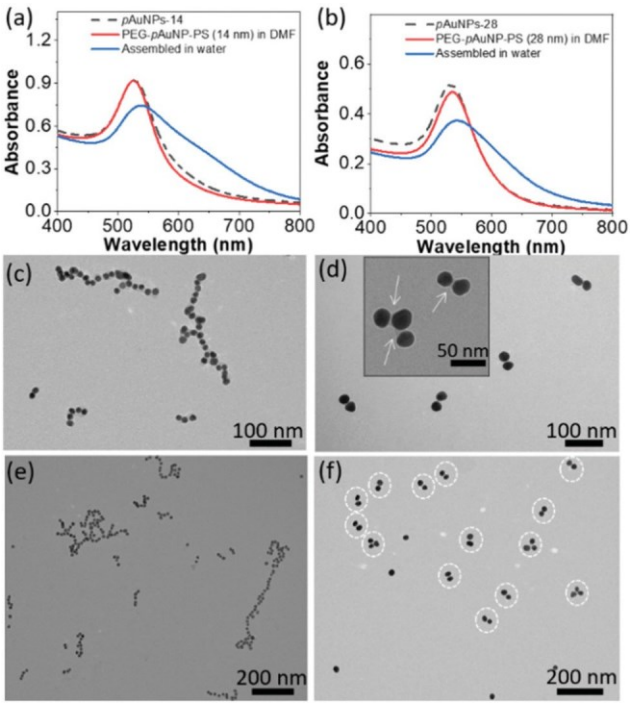


Fig. 5 UV-vis spectra of PEO-SH grafted 14 nm-pAuNP (a) and PEO-SH grafted 28.4 nm-pAuNP (b) assemblies. (c–f) TEM images at two different magnifications of PEO-SH grafted 14 nm-pAuNP (c and e) and PEO-SH grafted 28.4 nm-pAuNP assemblies (d and f).

## 3. Conclusions

In summary, we demonstrated the combined use of hydrophobicity-driven surface dewetting and seed-mediated growth to precisely pattern AuNPs with different surface coverage and topologically tune the asymmetric patches on AuNPs. The formation of Janus-type polymer patches was carried out under DLE conditions to produce high-quantity and water-soluble pAuNPs. Using the exposed surface on pAuNP-14 nm as seeds, we showed a highly controllable growth of AuNPs while retaining the size of polymer domains. The growth on pAuNPs could be extended to different metal precursors, like Ag, Pd and Pt, to yield A–B–C heterotrimers. As the freshly grown surface of AuNPs was covered by capping ligands, like CTAB, such surface anisotropy could further trigger the two-way self-assembly. By selective removal of CTAB, pAuNPs assembled along the exposed Au surfaces as the H–H assembly, driven by van de Waals interactions of uncovered Au surfaces. Reducing

the $A_c$ that increases the attractive interaction among pAuNPs resulted in clear morphological transitions from individual NPs to clusters and nanochains. Further modification of the exposed Au surface with $PEO_{44}$-SH could drive the T–T self-assembly where the hydrophobic PS collapsed in its non-solvent. We showed that the assembly modes played a key role in controlling the interparticle distance and therefore plasmon coupling of AuNPs.

Self-assembly of pAuNPs selectively grafted by amphiphile polymers, including linear block copolymers,[54–56] random copolymers,[57,58] and mixed homopolymer brushes,[51,59–61] has been demonstrated previously. The formation of Janus-type amphiphilic pAuNPs was usually carried out through selective surface modification templated by liquid–liquid[62,63] or solid–liquid[45,64] interfaces. A well-known example from Li et al. demonstrated the use of PEO-SH single crystals that physically adsorbed AuNPs to allow selective modification on the exposed surface with poly(methyl methacrylate). In spite of the directional interaction to guide the self-assembly, the balance of interparticle driving forces, i.e., the attractive interaction to drive self-assembly and the repulsive interaction to stabilize assembled nanostructures, has not been possible in previous designs. Combining the surface dewetting and seed-mediated growth, our strategy provides a clear solution to precisely design and essentially program the interparticle interaction. The current design allows us to not only control the directional self-assembly of pAuNPs in these two-way approaches, but also to precisely tune the interparticle interaction to vary the self-assembly nanostructures. Our results illustrate an alternative way for the directional self-assembly of anisotropic building blocks with great potential in programmable hierarchical assemblies. As an outcome, the two-way self-assembly of pAuNPs can tune the plasmon coupling strength. In the case of H–H self-assembly, the strongly coupled pAuNPs can be further used in sensing through surface enhanced Raman scattering (SERS) spectroscopy[65,66] and/or plasmon-enhanced photocatalysis.[67]

## Author contributions

H. D., Y. L. and J. H. conceived and designed the experiments. H. D., T. M., J. W., C.-H. L., and H. T. performed the experiments. H. D., M.-P. N, Y. L. and J. H. participated in discussions. The manuscript was drafted by H. D. and J. H. and all co-authors have contributed to revise and finalize the manuscript.

## Conflicts of interest

There are no conflicts to declare.

## Acknowledgements

J. H. is grateful for the support from the University of Connecticut, the Green Emulsions, Micelles and Surfactants (GEMS) Center, and the National Science Foundation (CBET-2102245). This study was also partially supported by the Institute of Materials Science at the University of Connecticut through the IMMP project. The TEM studies were performed using the facilities in the Bioscience Electron Microscopy Laboratory at the University of Connecticut and the Thermo Fisher Scientific Center for Advanced Microscopy and Materials Analysis (CAMMA).

## Notes and references

1 C. J. Murphy, T. K. Sau, A. M. Gole, C. J. Orendorff, J. Gao, L. Gou, S. E. Hunyadi and T. Li, J. Phys. Chem. B, 2005, 109, 13857–13870.
2 S. Panigrahi, S. Kundu, S. Ghosh, S. Nath and T. Pal, J. Nanopart. Res., 2004, 6, 411–414.
3 X. Yang, M. Yang, B. Pang, M. Vara and Y. Xia, Chem. Rev., 2015, 115, 10410–10488.
4 S. Gwo, H.-Y. Chen, M.-H. Lin, L. Sun and X. Li, Chem. Soc. Rev., 2016, 45, 5672–5716.
5 C. Yi, Y. Yang, B. Liu, J. He and Z. Nie, Chem. Soc. Rev., 2020, 49, 465–508.
6 Z. Li, Q. Fan and Y. Yin, Chem. Rev., 2022, 122, 4976–5067.
7 C. Yi, S. Zhang, K. T. Webb and Z. Nie, Acc. Chem. Res., 2017, 50, 12–21.
8 H. Duan, Y. Yang, Y. Zhang, C. Yi, Z. Nie and J. He, Giant, 2020, 4, 100033.
9 K. Yang, S. Zhang, J. He and Z. Nie, Nano Today, 2021, 36, 101046.
10 J. Lu, Y. Xue, K. Bernardino, N.-N. Zhang, W. R. Gomes, N. S. Ramesar, S. Liu, Z. Hu, T. Sun, A. F. de Moura, N. A. Kotov and K. Liu, Science, 2021, 371, 1368–1374.
11 K. Liu, Z. Nie, N. Zhao, W. Li, M. Rubinstein and E. Kumacheva, Science, 2010, 329, 197–200.
12 A. Klinkova, R. M. Choueiri and E. Kumacheva, Chem. Soc. Rev., 2014, 43, 3976–3991.
13 J. Kao, K. Thorkelsson, P. Bai, B. J. Rancatore and T. Xu, Chem. Soc. Rev., 2013, 42, 2654–2678.
14 S. Zhang, J. Chen, J. Liu, H. Pyles, D. Baker, C.-L. Chen and J. J. De Yoreo, Adv. Mater., 2021, 33, 1905784.
15 S. E. Skrabalak, Acc. Mater. Res., 2021, 2, 621–629.
16 S. C. Glotzer and M. J. Solomon, Nat. Mater., 2007, 6, 557–562.
17 M. R. Jones, R. J. Macfarlane, B. Lee, J. Zhang, K. L. Young, A. J. Senesi and C. A. Mirkin, Nat. Mater., 2010, 9, 913–917.
18 Z. J. Woessner and S. E. Skrabalak, J. Phys. Chem. C, 2021, 125, 23587–23596.
19 Y. Nagaoka, H. Zhu, D. Eggert and O. Chen, Science, 2018, 362, 1396–1400.
20 A. Kim, L. Yao, F. Kalutantirige, S. Zhou and Q. Chen, Self-Assembly of Nanostructures, IntechOpen, 2020.
21 Z. Zhang and S. C. Glotzer, Nano Lett., 2004, 4, 1407–1413.
22 S. Jiang, Q. Chen, M. Tripathy, E. Luijten, K. S. Schweizer and S. Granick, Adv. Mater., 2010, 22, 1060–1071.

 

23 Q. Chen, S. C. Bae and S. Granick, Nature, 2011, 469, 381–384.
24 Z. Nie, D. Fava, E. Kumacheva, S. Zou, G. C. Walker and M. Rubinstein, Nat. Mater., 2007, 6, 609–614.
25 A. Kim, S. Zhou, L. Yao, S. Ni, B. Luo, C. E. Sing and Q. Chen, J. Am. Chem. Soc., 2019, 141, 11796–11800.
26 J. Zhou, M. N. Creyer, A. Chen, W. Yim, R. P. M. Lafleur, T. He, Z. Lin, M. Xu, P. Abbasi, J. Wu, T. A. Pascal, F. Caruso and J. V. Jokerst, J. Am. Chem. Soc., 2021, 143, 12138–12144.
27 G. A. DeVries, M. Brunnbauer, Y. Hu, A. M. Jackson, B. Long, B. T. Neltner, O. Uzun, B. H. Wunsch and F. Stellacci, Science, 2007, 315, 358–361.
28 T. Chen, G. Chen, S. Xing, T. Wu and H. Chen, Chem. Mater., 2010, 22, 3826–3828.
29 G. Chen, K. J. Gibson, D. Liu, H. C. Rees, J.-H. Lee, W. Xia, R. Lin, H. L. Xin, O. Gang and Y. Weizmann, Nat. Mater., 2019, 18, 169–174.
30 C. A. Bohannon, A. J. Chancellor, M. T. Kelly, T. T. Le, L. Zhu, C. Y. Li and B. Zhao, J. Am. Chem. Soc., 2021, 143, 16919–16924.
31 T. Chen, M. Yang, X. Wang, L. H. Tan and H. Chen, J. Am. Chem. Soc., 2008, 130, 11858–11859.
32 R. M. Choueiri, E. Galati, H. Thérien-Aubin, A. Klinkova, E. M. Larin, A. Querejeta-Fernández, L. Han, H. L. Xin, O. Gang, E. B. Zhulina, M. Rubinstein and E. Kumacheva, Nature, 2016, 538, 79–83.
33 L. Yu, N. Zhang, N.-N. Zhang, Q. Gu, Y. Xue, Y.-X. Wang, C.-L. Han, K. Liu, Z.-Y. Sun, H.-J. Qian and Z.-Y. Lu, J. Phys. Chem. Lett., 2021, 12, 7100–7105.
34 Y. Yang, C. Yi, X. Duan, Q. Wu, Y. Zhang, J. Tao, W. Dong and Z. Nie, J. Am. Chem. Soc., 2021, 143, 5060–5070.
35 B. Liu, S. Thanneeru, A. Lopes, L. Jin, M. McCabe and J. He, Small, 2017, 13, 1700091.
36 H. Duan, Q. Luo, Z. Wei, Y. Lin and J. He, ACS Macro Lett., 2021, 10, 786–790.
37 D. Gentili, G. Foschi, F. Valle, M. Cavallini and F. Biscarini, Chem. Soc. Rev., 2012, 41, 4430–4443.
38 F. Liu, S. Goyal, M. Forrester, T. Ma, K. Miller, Y. Mansoorieh, J. Henjum, L. Zhou, E. Cochran and S. Jiang, Nano Lett., 2018, 19, 1587–1594.
39 W. Li, S. Ravaine and E. Duguet, J. Colloid Interface Sci., 2020, 560, 639–648.
40 J. Reguera, T. Flora, N. Winckelmans, J. C. Rodríguez-Cabello and S. Bals, Nanoscale Adv., 2020, 2, 2525–2530.
41 N. R. Jana, L. Gearheart and C. J. Murphy, Langmuir, 2001, 17, 6782–6786.
42 W. Haiss, N. T. Thanh, J. Aveyard and D. G. Fernig, Anal. Chem., 2007, 79, 4215–4221.
43 J. Feng, D. Xu, F. Yang, J. Chen, C. Wu and Y. Yin, Angew. Chem., Int. Ed., 2021, 60, 16958–16964.
44 J. Qiu, Q. N. Nguyen, Z. Lyu, Q. Wang and Y. Xia, Adv. Mater., 2021, 2102591.
45 J. Qiu, M. Xie, Z. Lyu, K. D. Gilroy, H. Liu and Y. Xia, Nano Lett., 2019, 19, 6703–6708.
46 J. Li, Y. Zheng, J. Zeng and Y. Xia, Chem. – Eur. J., 2012, 18, 8150–8156.
47 H. Ataee-Esfahani, L. Wang, Y. Nemoto and Y. Yamauchi, Chem. Mater., 2010, 22, 6310–6318.
48 H. Hu, F. Ji, Y. Xu, J. Yu, Q. Liu, L. Chen, Q. Chen, P. Wen, Y. Lifshitz and Y. Wang, ACS Nano, 2016, 10, 7323–7330.
49 P. K. Jain, W. Huang and M. A. El-Sayed, Nano Lett., 2007, 7, 2080–2088.
50 M. K. Corbierre, N. S. Cameron, M. Sutton, K. Laaziri and R. B. Lennox, Langmuir, 2005, 21, 6063–6072.
51 B. Wang, B. Li, B. Zhao and C. Y. Li, J. Am. Chem. Soc., 2008, 130, 11594–11595.
52 R. M. Choueiri, A. Klinkova, H. s. Thérien-Aubin, M. Rubinstein and E. Kumacheva, J. Am. Chem. Soc., 2013, 135, 10262–10265.
53 W. Li, I. Kanyo, C.-H. Kuo, S. Thanneeru and J. He, Nanoscale, 2015, 7, 956–964.
54 E. R. Zubarev, J. Xu, A. Sayyad and J. D. Gibson, J. Am. Chem. Soc., 2006, 128, 15098–15099.
55 J. He, Y. Liu, T. Babu, Z. Wei and Z. Nie, J. Am. Chem. Soc., 2012, 134, 11342–11345.
56 J. He, X. Huang, Y.-C. Li, Y. Liu, T. Babu, M. A. Aronova, S. Wang, Z. Lu, X. Chen and Z. Nie, J. Am. Chem. Soc., 2013, 135, 7974–7984.
57 C. Yi, H. Liu, S. Zhang, Y. Yang, Y. Zhang, Z. Lu, E. Kumacheva and Z. Nie, Science, 2020, 369, 1369–1374.
58 C. Yi, Y. Yang and Z. Nie, J. Am. Chem. Soc., 2019, 141, 7917–7925.
59 B. Wang, B. Li, B. Dong, B. Zhao and C. Y. Li, Macromolecules, 2010, 43, 9234–9238.
60 J. Song, L. Cheng, A. Liu, J. Yin, M. Kuang and H. Duan, J. Am. Chem. Soc., 2011, 133, 10760–10763.
61 J. Song, J. Zhou and H. Duan, J. Am. Chem. Soc., 2012, 134, 13458–13469.
62 E. Glogowski, J. He, T. P. Russell and T. Emrick, Chem. Commun., 2005, 4050–4052, DOI: 10.1039/B503670D.
63 H.-Y. Lee, S. H. R. Shin, L. L. Abezgauz, S. A. Lewis, A. M. Chirsan, D. D. Danino and K. J. Bishop, J. Am. Chem. Soc., 2013, 135, 5950–5953.
64 A. Ohnuma, E. C. Cho, P. H. Camargo, L. Au, B. Ohtani and Y. Xia, J. Am. Chem. Soc., 2009, 131, 1352–1353.
65 G. Chen, Y. Wang, M. Yang, J. Xu, S. J. Goh, M. Pan and H. Chen, J. Am. Chem. Soc., 2010, 132, 3644–3645.
66 R. Zhu, H. Feng, Q. Li, L. Su, Q. Fu, J. Li, J. Song and H. Yang, Angew. Chem., 2021, 133, 12668–12676.
67 S. K. Cushing, J. Li, F. Meng, T. R. Senty, S. Suri, M. Zhi, M. Li, A. D. Bristow and N. Wu, J. Am. Chem. Soc., 2012, 134, 15033–15041.